Supporting information

Amorphization driven Na-Alloying in Si_xGe_{1-x} alloy nanowires for Na-ion battery

Syed Abdul Ahad, Seamus Kilian, Maria Zubair, Vasily A. Lebedev, Karrina McNamara, Kevin M. Ryan, Tadhg Kennedy, Hugh Geaney *

Department of Chemical Sciences and Bernal Institute, University of Limerick, Limerick V94 T9PX, Ireland

**Corresponding author: Hugh Geaney, Department of Chemical Sciences and Bernal Institute, University of Limerick, Limerick V94 T9PX, Ireland, Email: Hugh.Geaney@ul.ie*

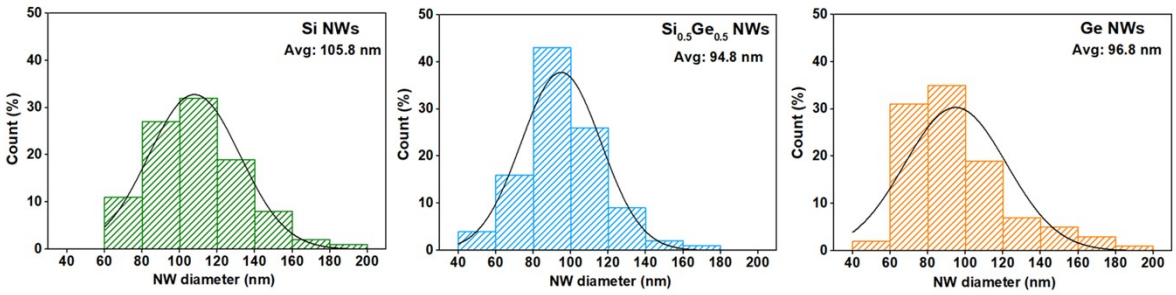

Fig S1. Histogram of diameter distribution of Si, $Si_{0.5}Ge_{0.5}$ and Ge NWs respectively

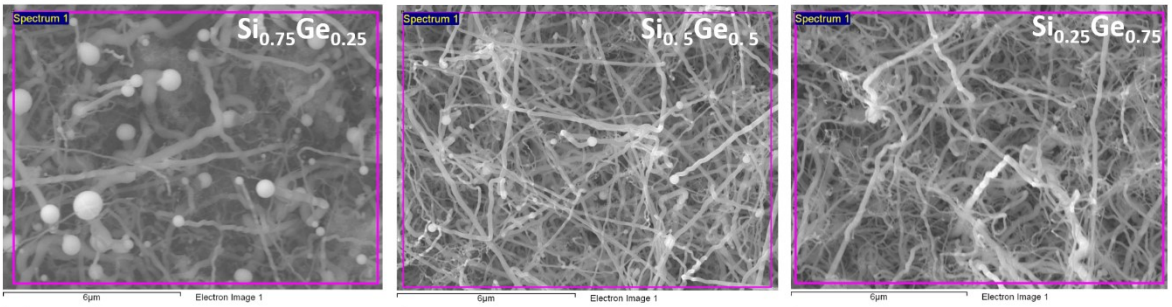

Spectrum processing :
Peaks possibly omitted : 2.301, 5.414, 5.931, 6.401, 7.055, 7.472, 8.264 keV

Processing option : All elements analyzed (Normalised)
Number of iterations = 3

Standard :
Si SiO2 1-Jun-1999 12:00 AM
Ge Ge 1-Jun-1999 12:00 AM
Sn Sn 1-Jun-1999 12:00 AM

Element	Weight%	Atomic%
Si K	43.28	68.92
Ge K	40.64	25.02
Sn L	16.08	6.06
Totals	100.00	

Spectrum processing :
Peaks possibly omitted : 2.302, 5.415, 5.928, 6.400, 7.055, 7.471, 8.260 keV

Processing option : All elements analyzed (Normalised)
Number of iterations = 3

Standard :
Si SiO2 1-Jun-1999 12:00 AM
Ge Ge 1-Jun-1999 12:00 AM
Sn Sn 1-Jun-1999 12:00 AM

Element	Weight%	Atomic%
Si K	25.48	48.34
Ge K	63.84	46.86
Sn L	10.69	4.80
Totals	100.00	

Spectrum processing :
Peaks possibly omitted : 2.296, 5.416, 5.934, 6.400, 7.054, 7.473, 8.263 keV

Processing option : All elements analyzed (Normalised)
Number of iterations = 3

Standard :
Si SiO2 1-Jun-1999 12:00 AM
Ge Ge 1-Jun-1999 12:00 AM
Sn Sn 1-Jun-1999 12:00 AM

Element	Weight%	Atomic%
Si K	11.21	25.43
Ge K	79.18	69.42
Sn L	9.61	5.16
Totals	100.00	

Fig S2. EDS data of $Si_{0.75}Ge_{0.25}$, $Si_{0.5}Ge_{0.5}$ and $Si_{0.25}Ge_{0.75}$ NWs with corresponding atomic and weight ratios of Si, Ge and Sn.

Please note that the above listed compositions contain 4-6 at. % Sn as well which is coming from 20 nm Sn seed catalyst used to grow Si_xGe_{1-x} NWs using SLS method. Therefore, the complete nomenclature of these compositions can be written as $Si_{0.6892}Ge_{0.2502}Sn_{0.0606}$, $Si_{0.4834}Ge_{0.4686}Sn_{0.0480}$ and $Si_{0.2545}Ge_{0.6942}Sn_{0.0516}$. However, for simplicity, the compositions are listed based on the nearest Si and Ge composition such as $Si_{0.75}Ge_{0.25}$, $Si_{0.5}Ge_{0.5}$ and $Si_{0.25}Ge_{0.75}$ respectively.

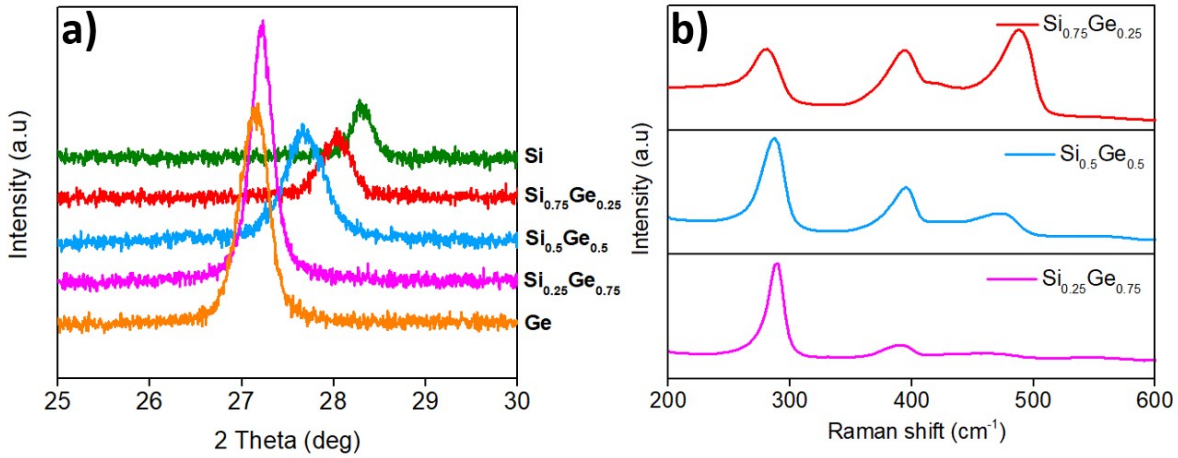

Fig S3. (a) XRD analysis of different alloy compositions, pure Si and pure Ge phases between 25° – 30° to show clear shift in (111) peak shift. (b) Raman spectra of different alloy compositions and the corresponding shift in Si-Si, Si-Ge and Ge-Ge active modes.

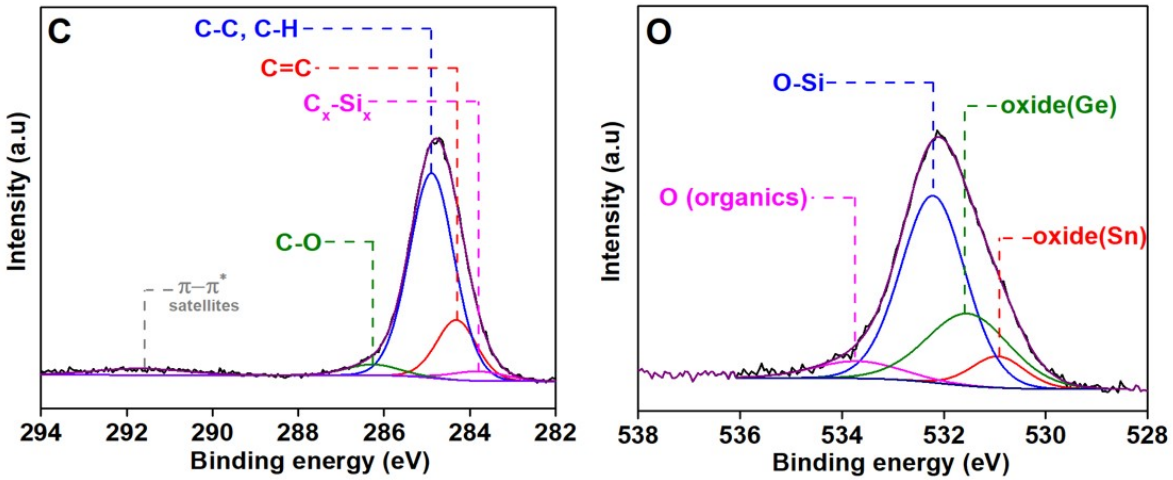

Fig S4. XPS core-level spectra of C and O of $Si_{0.5}Ge_{0.5}$ NW.

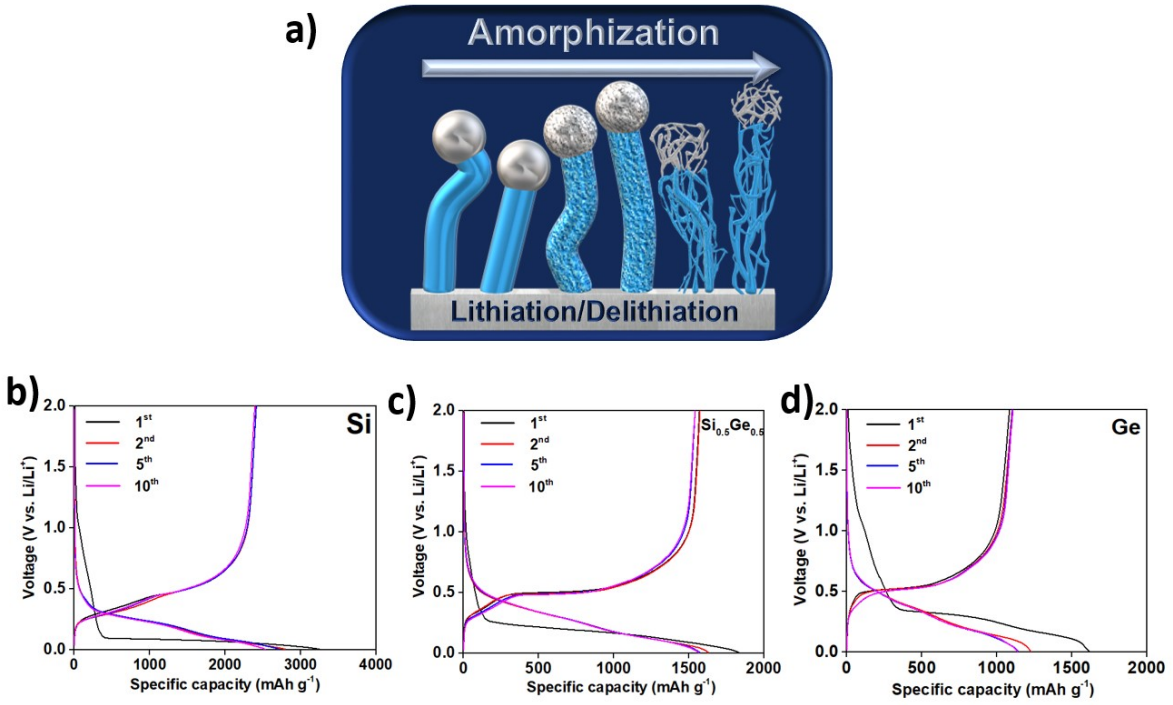

Fig S5. (a) Schematic illustration of amorphization step of crystalline NW in a LIB. Voltage-capacity profile of (a) Si, (b) $Si_{0.5}Ge_{0.5}$ and (c) Ge NWs cycled in a LIB between 0.005-2.0 V at C/5 rate.

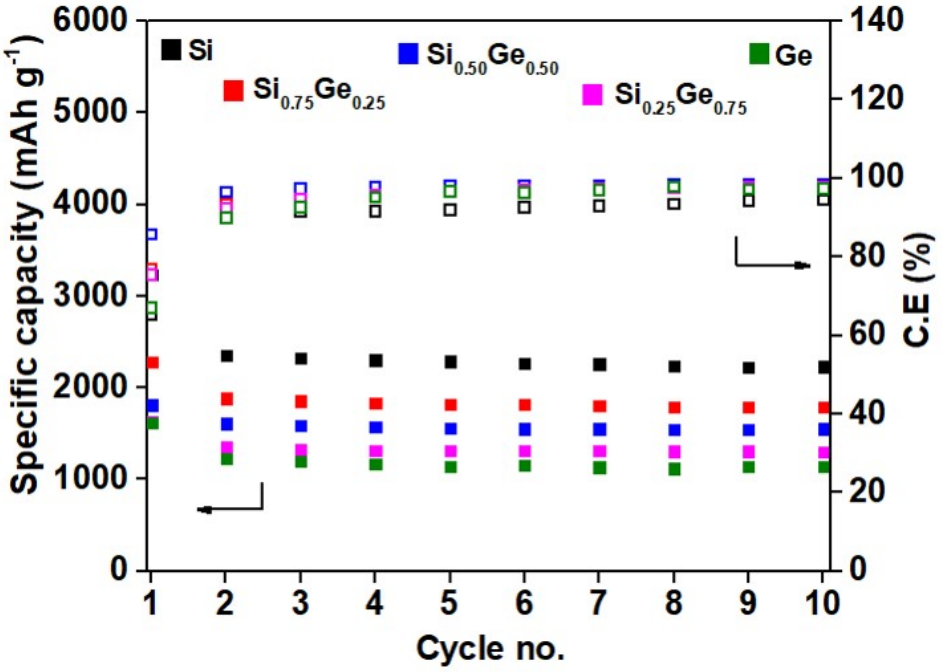

Fig S6. Cyclic performance of pure Si, pure Ge and different Si_xGe_{1-x} alloy NW compositions cycled in a LIB between 0.005 – 2.0 V at C/5 rate.

The first cycle lithiation capacity obtained was 3231.1 mAh g^{-1}, 2282 mAh g^{-1}, 1811.8 mAh g^{-1} , 1630.95 mAh g^{-1} and 1615.3 mAh g^{-1} for Si, $Si_{0.75}Ge_{0.25}$, $Si_{0.5}Ge_{0.5}$, $Si_{0.25}Ge_{0.75}$ and Ge respectively which included 1st cycle lithiation as well as capacity derived from the formation of solid-electrolyte interface (SEI) layer. Subsequently after 10 cycles, lithiation capacity was 2228.85 mAh g^{-1}, 1788.64 mAh g^{-1}, 1550.25 mAh g^{-1}, 1301.96 mAh g^{-1} and 1137.77 mAh g^{-1} for Si, $Si_{0.75}Ge_{0.25}$, $Si_{0.50}Ge_{0.50}$, $Si_{0.25}Ge_{0.75}$ and Ge respectively, with coulombic efficiency ranging from 94 % – 97 % for all the alloys and parent phases. The slightly lower specific capacity obtained in the subsequent cycles might be due to the irreversible alloying with the oxide species, also highlighted in XPS analysis (**Figure 2f-h**).[1]

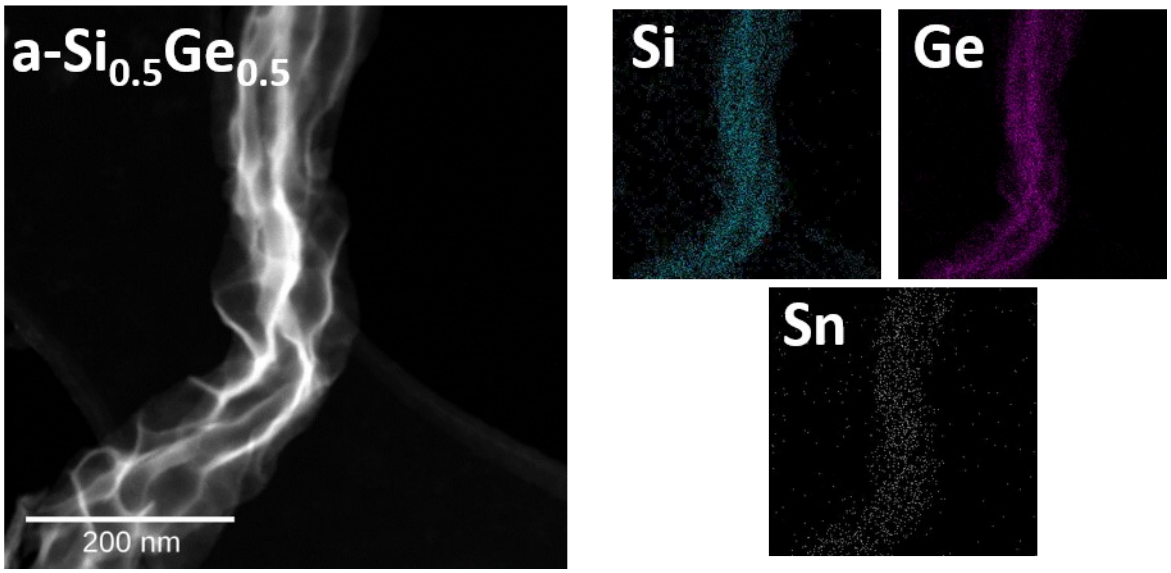

Fig S7. STEM image and corresponding EDX mapping of Si, Ge and Sn elemental distribution in de-lithiated $Si_{0.5}Ge_{0.5}$ NW.

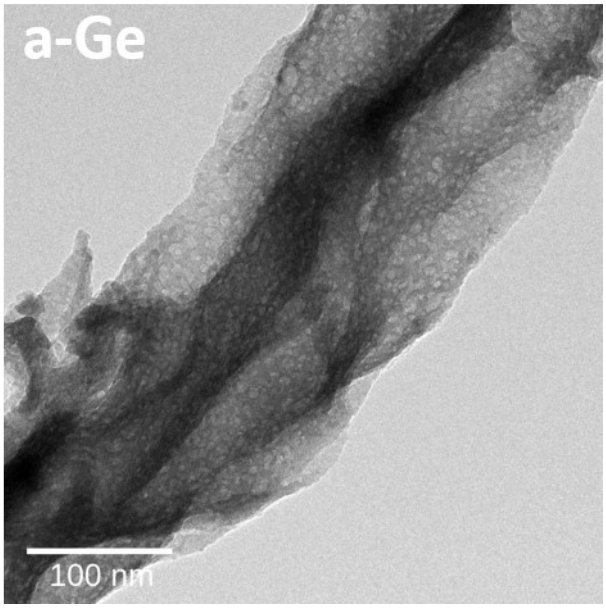

Fig S8. High magnification TEM image showing nanopores in de-lithiated a-Ge NW.

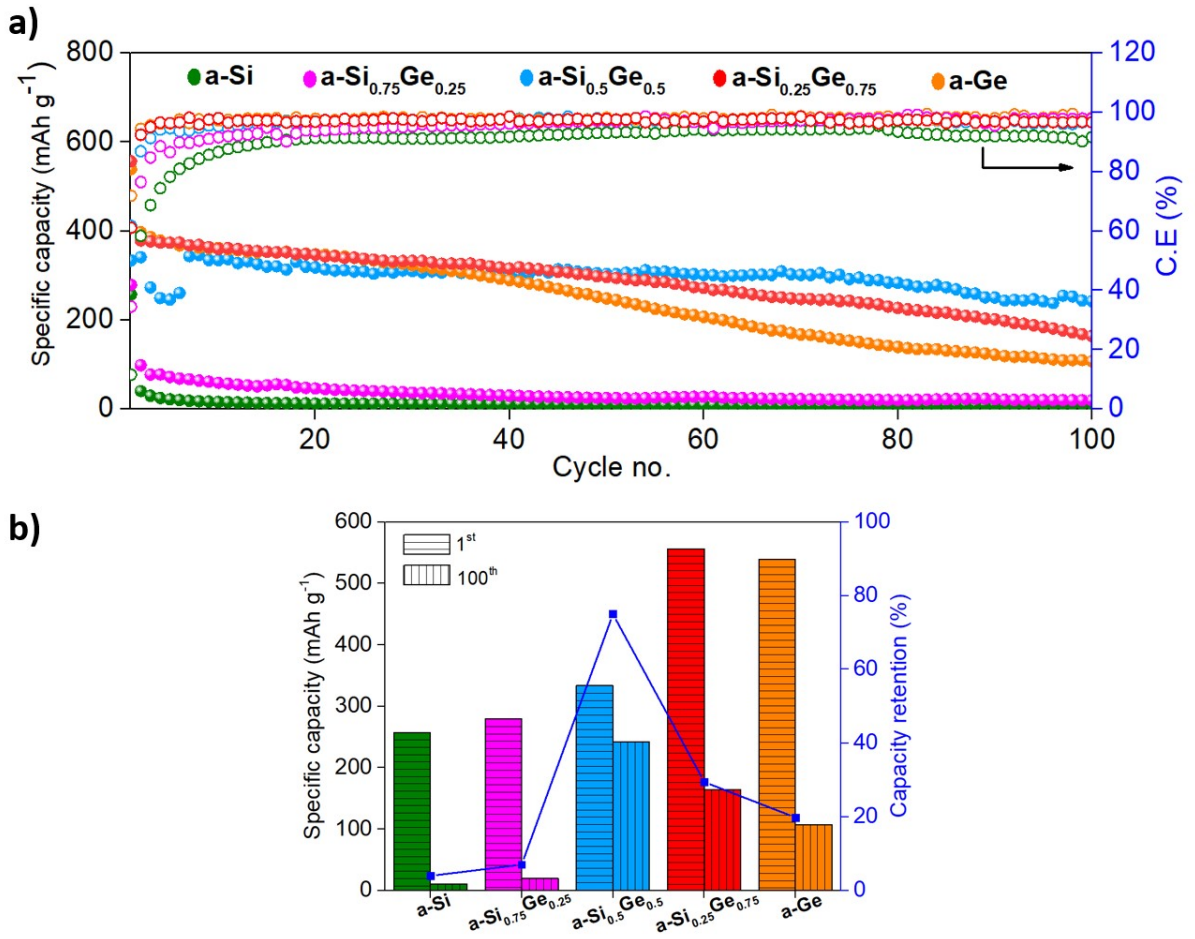

Fig S9. (a) Specific capacity vs. cycle no. and (b) Comparison of specific capacity retention between 1st and 100th cycle of a-Si, a-Ge and various a-Si$_x$Ge$_{1-x}$ alloy compositions cycled between 0.005-2.0 V at 50 mA g^{-1}. The capacity retention after 100 cycles for a-Si, a-Si$_{0.75}$Ge$_{0.25}$, a-Si$_{0.5}$Ge$_{0.5}$, a-Si$_{0.75}$Ge$_{0.25}$ and a-Ge was 3.93%, 7.0%, 75%, 29.4% and 19.8% respectively.

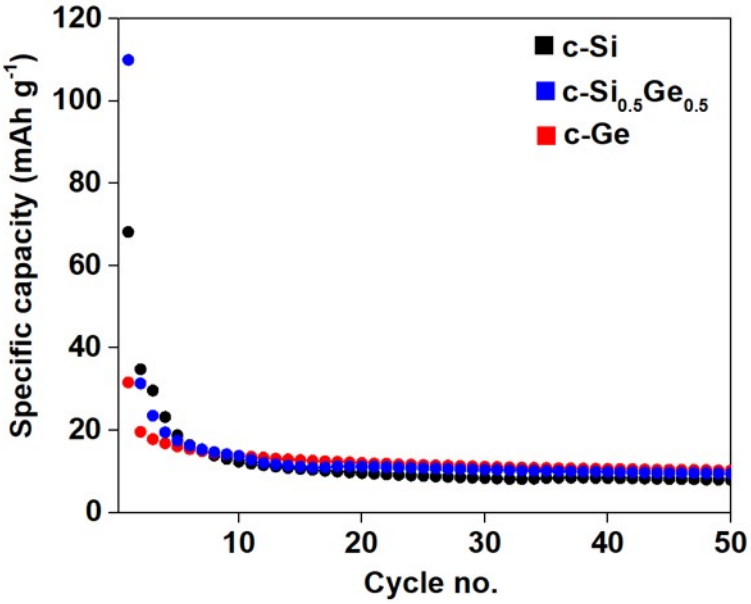

Fig S10. Specific capacity vs. cycle no. of c-Si, c-Si0.5Ge0.5 and c-Ge cycled between 0.005-2.0 V at 50 mA g^{-1} in a NIB.

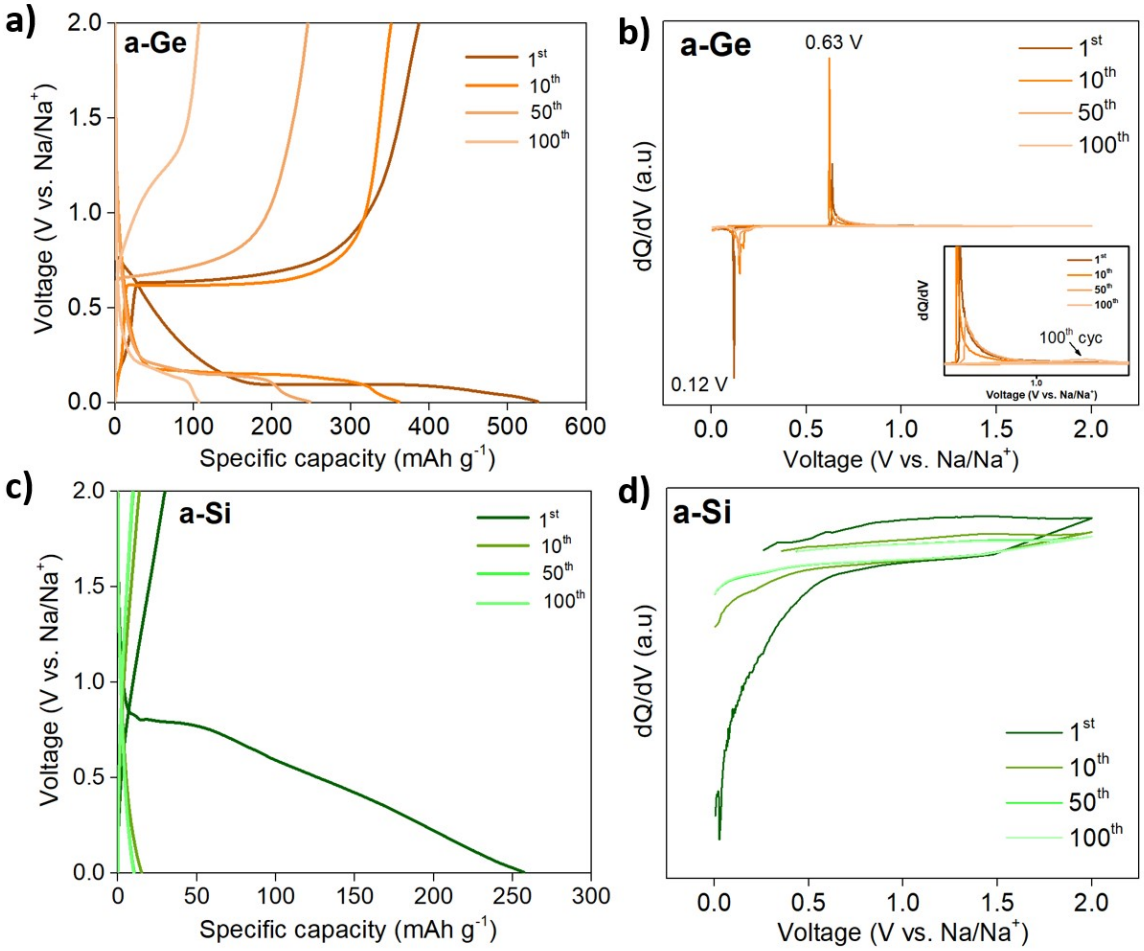

Fig S11. Voltage - capacity profile (a,c) and corresponding differential-capacity plot (b,d) of a-Ge and a-Si cycled between 0.005 – 2.0 V.

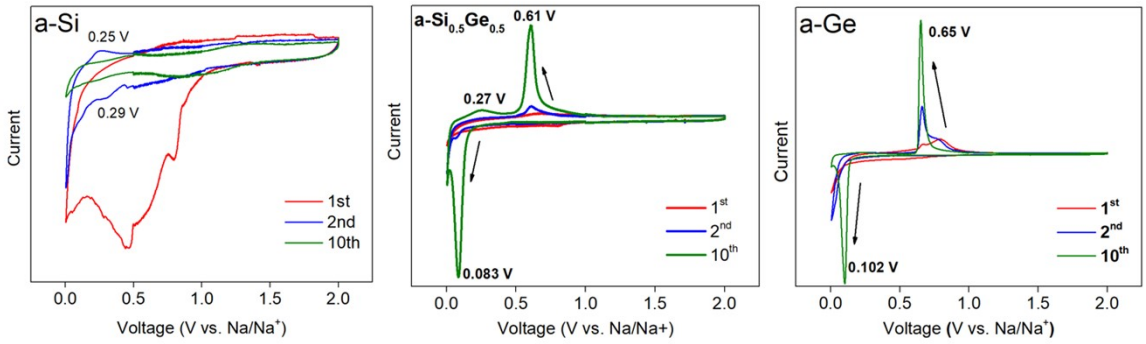

Fig S12. Cyclic voltammetry graphs of a-Si, a-$Si_{0.5}Ge_{0.5}$ and a-Ge at a scan rate of 0.02 mV s^{-1}.

The CV plots showed that after the 1st cycle, there is a broad peak around 0.29 V, consistent with Na intercalation in a-Si while the broad peak around 0.25 V can be attributed to the desodiation of Na ion from a-Si.[2] However, in the subsequent cycles, these peaks completely disappear, suggesting irreversible sodium insertion in the a-Si structure. The sodiation peaks appear at 0.083 and 0.102 V while the desodiation peaks appear at 0.61 V and 0.65 V for a-$Si_{0.5}Ge_{0.5}$ and a-Ge respectively after 10 cycles. These results agree with the differential capacity plots presented in Fig 4d and Fig S11b. A broad peak appearing at 0.27 V for a-$Si_{0.5}Ge_{0.5}$ might be due to the desodiation of Na_xSn or Na_xSi phase. However, no sodiation peaks were found which could be attributed to the formation of Na_ySn phase.

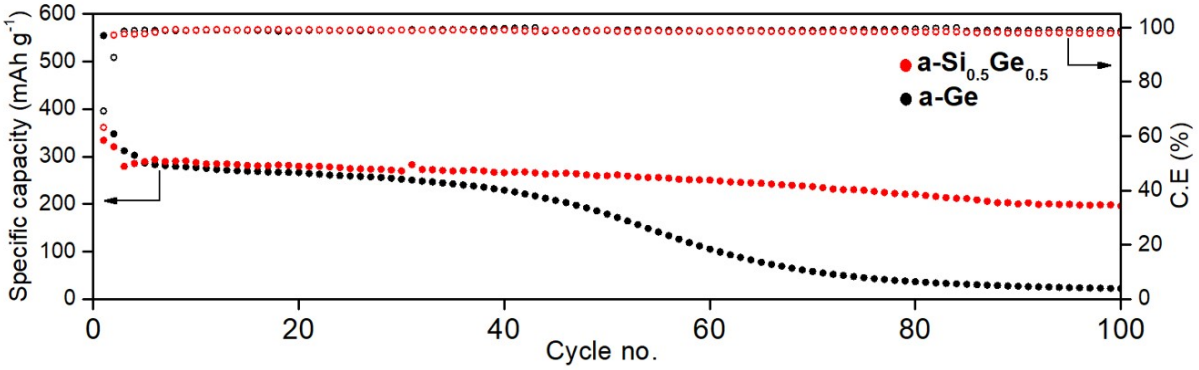

Fig S13. (a) Specific capacity vs. cycle no. of a-$Si_{0.5}Ge_{0.5}$ and a-Ge NWs cycled between 0.005-2.0 V at 200 mA g^{-1}.

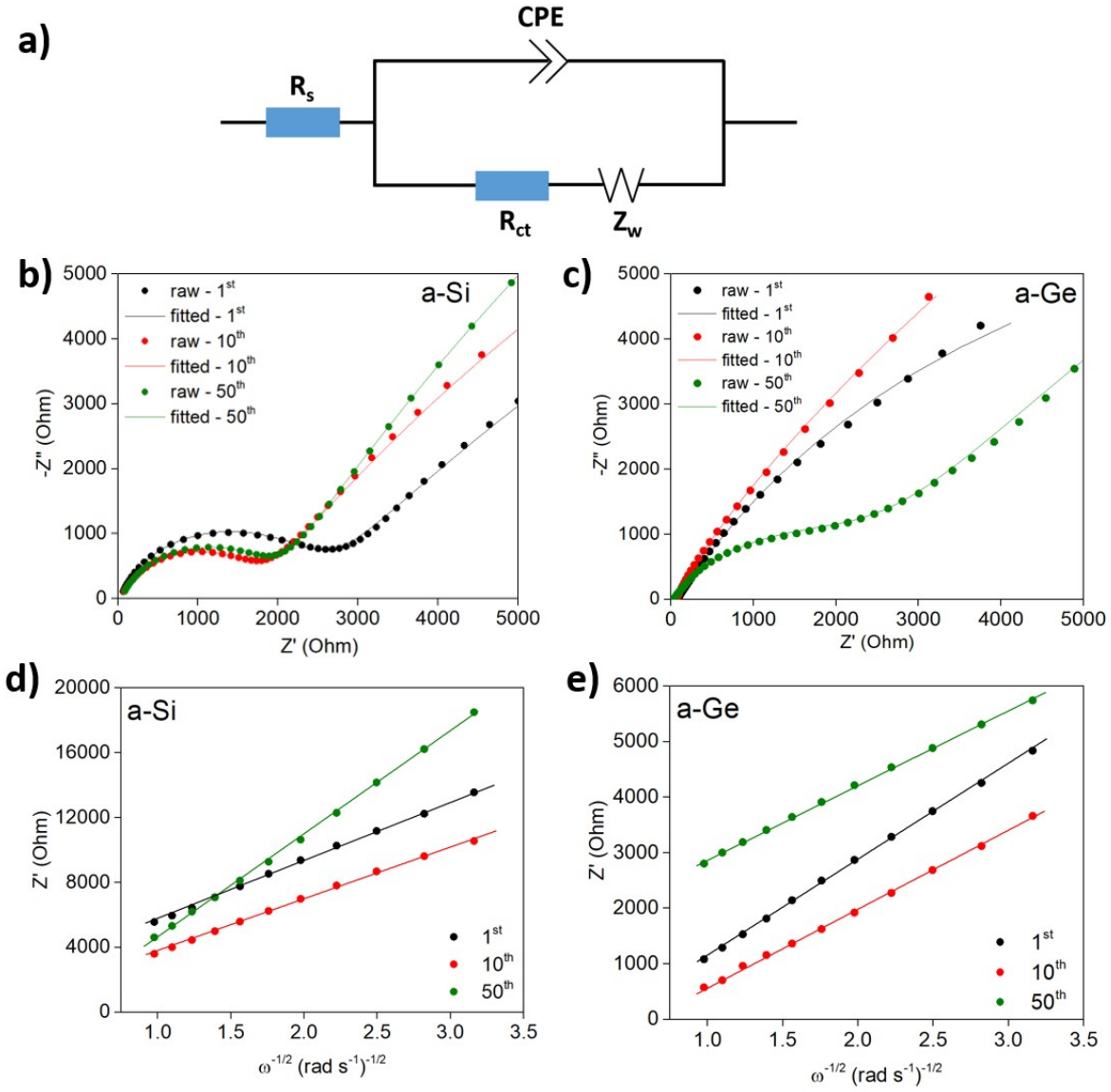

Fig S14 (a) Equivalent circuit used for fitting of EIS data. The Nyquist plots of a-Si (b) and a-Ge (c) after 1st, 10th and 50th cycle. The Z vs. w-1/2 plots of a-Si (d) and a-Ge (e) derived from their corresponding Nyquist plots.

The equivalent circuit contains R_s which is the solution resistance of the cell, R_{ct} is the charge transfer resistance, CPE is the capacitance while Z_w is the Warburg factor.

	a-Si		$a\text{-}Si_{0.5}Ge_{0.5}$		a-Ge	
	R_s (Ohm)	R_{ct} (Ohm)	R_s (Ohm)	R_{ct} (Ohm)	R_s (Ohm)	R_{ct} (Ohm)
1st	33.03	2537	26.25	1681	33	49.48
10th	39.71	1813	26.33	909.5	33.5	44.65
50th	40.48	2014	29.33	235.6	39.7	2892

Table S1. Tabulation of R_s and R_{ct} value of a-Si, $a\text{-}Si_{0.5}Ge_{0.5}$ and a-Ge at different cycle no. cycled in a NIB.

	a-Si		$a\text{-}Si_{0.5}Ge_{0.5}$		a-Ge	
	D_{Na} ($cm^2\ s^{-1}$)	σ	D_{Na} ($cm^2\ s^{-1}$)	σ	D_{Na} ($cm^2\ s^{-1}$)	σ
1st	3.72×10^{-18}	3764.2	7.65×10^{-18}	2623.3	17.70×10^{-18}	1722.9
10th	4.37×10^{-18}	3473.6	19.19×10^{-18}	1657.1	26.71×10^{-18}	1404.7
50th	1.29×10^{-18}	6382.7	19.78×10^{-18}	1632.2	28.65×10^{-18}	1356.31

Table S2. Tabulation of corresponding σ and D_{Na} values of a-Si, $a\text{-}Si_{0.5}Ge_{0.5}$ and a-Ge at different cycle no. cycled in a NIB.

The values of σ and D_{Na} were calculated from the following equation:

Equation 1 → $D_{Na^+} = R^2\,T^2 / 2n^4\,F^4\,A^2\,C^2\,\sigma^2$

Equation 2 → $Z' = R_s + R_{ct} + \sigma\omega^{-1/2}$

Where D_{Na}^{+}, R, T, n, A, F, C and σ are Na ion Diffusion coefficient, gas constant, temperature, no. of electrons per molecule during oxidation, surface area of electrode, Faraday constant, Na ion concentration and Warburg factor (calculated using Eq. 1) respectively.

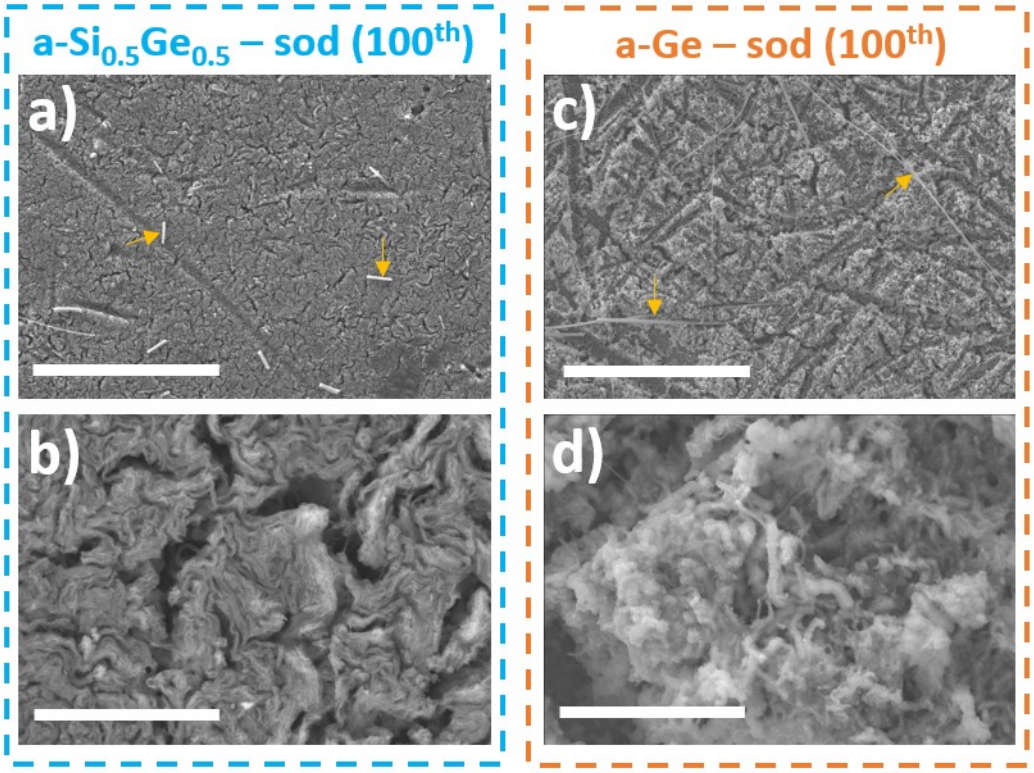

Fig S15. SEM image of (a, b) a-$Si_{0.5}Ge_{0.5}$ -sodiated and (c, d) a-Ge – sodiated state after 100th cycle. The scale bares in a, & c represents 50 µm while scale bar in b & d represents 5 µm. The orange arrows indicate glass fibers remains from the GF/D current collector after cell disassembly.

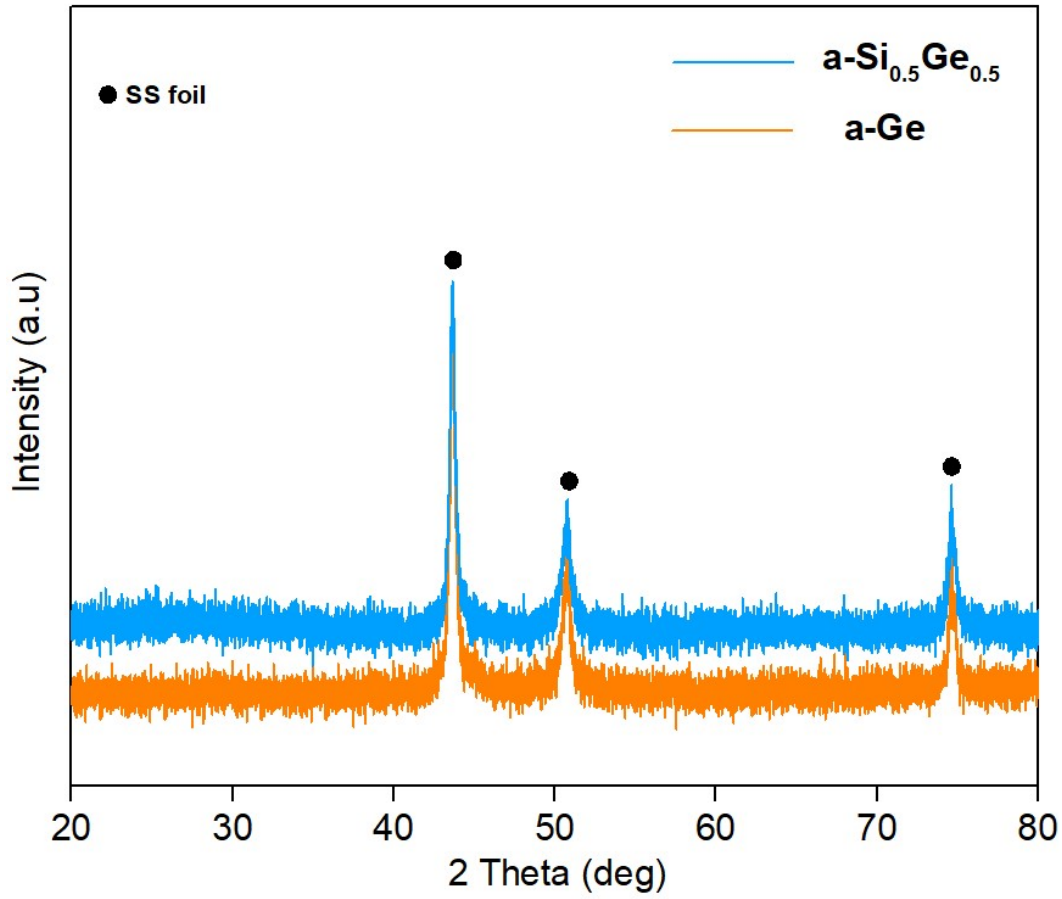

Fig S16. Post-mortem XRD analysis of a- $Si_{0.5}Ge_{0.5}$ and a-Ge NW post Na-ion cycling.

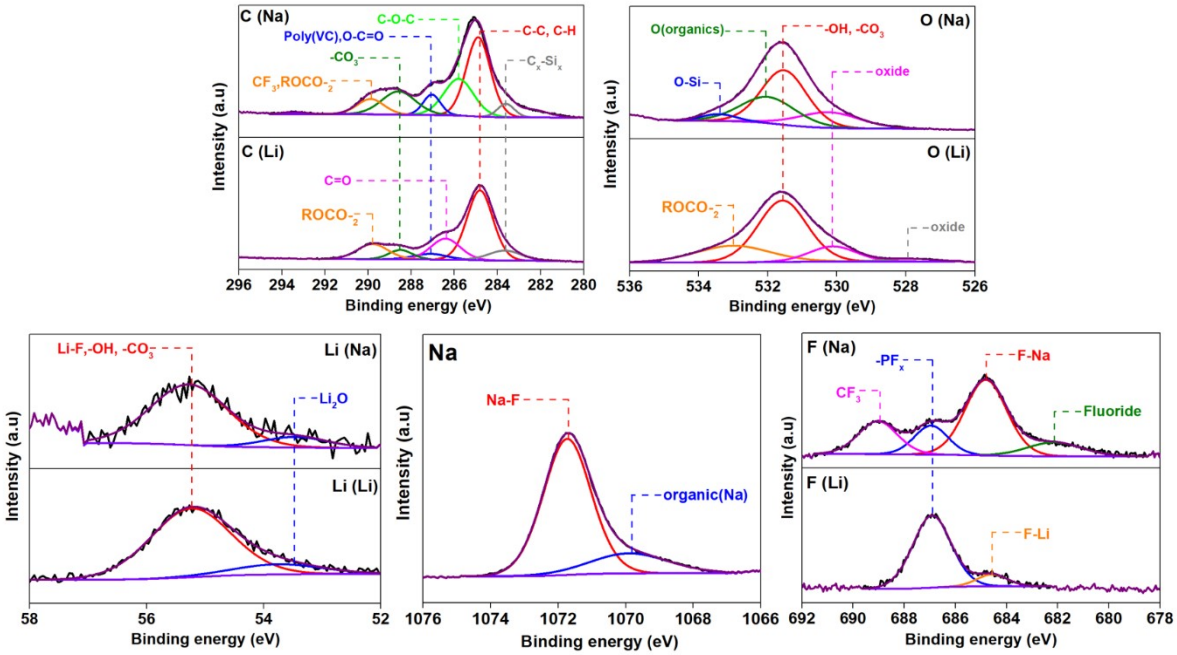

Fig S17. XPS core-level spectra of C, O, Li, Na and F in delithiated (represented by (Li)) and desodiated (represented by (Na)) state of a-$Si_{0.5}Ge_{0.5}$ NW.

A comparison of the C 1s spectra shows the typical presence of organic/inorganic species like C-C, -O-C=O (ester), C=O, C-O-C (ether), $ROCO_2$-, CO_3- (Li, Na) and CF_3 from decomposition of $LiPF_6$ and NaOTf salt. The O 1s spectra also shows the presence of mostly organic oxide species, corresponding to the species shown in C 1s spectra. The Li (Li) spectra reveals the presence of LiF, $LiCO_3$ and oxide species due to the decomposition of $LiPF_6$ salt and additives involved in the electrolyte. Finally apart from Na-organics presence, the Na spectra reveals the additional formation of NaF and CF_3 species from the decomposition of NaOTf salt while still showing the LiF and other Li-based inorganic species suggesting that SEI formed due to earlier lithiation/delithiation co-exists with SEI formed due to sodiation/desodiation process. Lastly, F 1s spectra confirms the presence of organic/inorganic based –F species (i.e. LiF, NaF, $-CF_3$, PF_x and fluorides from decomposed electrolyte salt) from both the delithiated and desodiated state of a-$Si_{0.5}Ge_{0.5}$ NW.[3,4,5]

References

1 M. T. McDowell, S. W. Lee, I. Ryu, H. Wu, W. D. Nix, J. W. Choi and Y. Cui, *Nano Lett.*, 2011, **11**, 4018.

2 S. Huang, L. Liu, Y. Zheng, Y. Wang, D. Kong, Y. Zhang, Y. Shi, L. Zhang, O. G. Schmidt and H. Y. Yang, *Adv. Mater.*, 2018, **30**, 1706637.

3 T. Kennedy, M. Brandon, F. Laffir and K. M. Ryan, *J. Power Sources*, 2017, **359**, 601.

4 P. M. L. Le, T. D. Vo, H. Pan, Y. Jin, Y. He, X. Cao, H. V. Nguyen, M. H. Engelhard, C. Wang, J. Xiao and J. G. Zhang, *Adv. Funct. Mater.*, 2020, **30**, 2001151.

5 G. G. Eshetu, T. Diemant, M. Hekmatfar, S. Grugeon, R. J. Behm, S. Laruelle, M. Armand and S. Passerini, *Nano Energy*, 2019, **55**, 327–340.